

---

# Data-Efficient Mutual Information Neural Estimator

---

**Xiao Lin<sup>1\*</sup>, Indranil Sur<sup>1\*</sup>, Samuel A. Nastase<sup>2</sup>,  
Ajay Divakaran<sup>1</sup>, Uri Hasson<sup>2</sup> and Mohamed R. Amer<sup>1</sup>**  
<sup>1</sup>SRI International, Princeton, NJ, USA    <sup>2</sup>Princeton University, Princeton, NJ, USA

## Abstract

Measuring Mutual Information (MI) between high-dimensional, continuous, random variables from observed samples has wide theoretical and practical applications. While traditional MI methods, such as [32], capable of capturing MI between low-dimensional signals, they fall short when dimensionality increases and are not scalable. Existing neural approaches, such as [5], searches for a  $d$ -dimensional neural network that maximizes a variational lower bound for mutual information estimation; however, this requires  $O(d \log d)$  observed samples to prevent the neural network from overfitting. For practical mutual information estimation in real world applications, data is not always available at a surplus, especially in cases where acquisition of the data is prohibitively expensive, for example in fMRI analysis. We introduce a scalable, data-efficient mutual information estimator. By coupling a learning-based view of the MI lower bound with meta-learning, DEMINE achieves high-confidence estimations irrespective of network size and with improved accuracy at practical dataset sizes. We demonstrate the effectiveness of DEMINE on synthetic benchmarks as well as a real world application of fMRI inter-subject correlation analysis.

## 1 Introduction

Mutual Information (MI) is one of the most important, theoretically grounded, measures of similarity between random variables. MI captures non-linear statistical dependencies between random variables. It is widely used quantity in various machine learning tasks ranging from classification to feature selection and clustering. Traditional approaches used binning [15, 9], entropy estimation from k-nearest neighbor distances [32] making them data efficient, adaptive with minimal bias, however, when it came to large dimensionality these methods fail to scale. In high dimensional, continuous spaces, such as text, images, videos, fMRI and other time-series signals, measuring mutual information between random variables is prohibitively expensive and complex computation.

With the success of neural networks capturing similarity in representations and distributions of large dimensional spaces, a new Mutual Information Neural Estimator (MINE) was proposed [5]. Similar to Generative Adversarial Networks (GANs) [20] estimating an implicit density using Kullback-Leibler (KL) divergence without any assumptions about the distributions, MINE uses KL-divergence, and cast the estimation in the same framework as  $f$ -divergences using a dual formulation [35]. Compared to traditional methods, MINE is scalable, flexible and optimized using back-propagation.

In this work, inspired by recent successes of [5], we propose a new measure that utilizes neural networks, Neural Mutual Information (DEMINE). Our approach diverges from [5] by training a neural network to predict mutual information on a seen dataset and estimate if on an unseen dataset which avoids overfitting and is applicable to high dimensional datasets, with small number of instances. We validate and apply DEMINE to more complex problem, that of capturing brain-to-brain coupling in functional Magnetic Resonance Imaging (fMRI) data. DEMINE captures distributed, nonlinear inter-subject coupling by learning to predict the lower bound of mutual information between

---

\* equal contribution

spatio-temporal fMRI responses across individuals. In brief, by using neural networks to encode continuous fMRI responses, we can learn nonlinear and higher-order inter-subject associations.

With the success of Meta-Learning [11], in improve the generalization capability model by learning better hyperparameters, network architectures, initialization, and loss functions. We develop a new meta-learning framework for mutual information estimation, Meta-DEMINE. We developed a task augmentation approach by utilizing MI’s invariance to invertible transformations which makes meta-learning less prone to overfitting.

Our contributions are summarized as:

- Data efficient neural mutual information estimator (DEMINE)
- New formulation of meta learning using Task Augmentation (Meta-DEMINE)
- Application to real life, data scarce, application (fMRI)

## 2 Related Work

In this section we review relevant literature for mutual information estimation and meta learning.

**Mutual information estimation.** The standard approach for estimating mutual information between two continuous random variables from samples has been using k-NN estimates, notably the KSG estimator [32]. Recent works [17] have provided a comprehensive review and studied the consistency and of asymptotic confidence bound of the KSG estimator [18]. Mutual information estimation can also be achieved by estimating the individual entropy terms involved through kernel density estimation [2], or by estimating cross-entropy [34]. Overfitting can be reduced through partitioning the samples into different folds for modeling and for estimation. Despite of their fast and accurate estimations on random variables with few dimensions, mutual information estimating on high-dimensional random variables remains challenging for commonly used Gaussian kernels.

Fundamentally, estimating mutual information requires the ability to accurately model the random variables, where high-capacity neural networks have shown excellent performance for modeling complex high-dimensional signals such as image and sound. The IM algorithm [1] introduces a variational mutual information lower bound, where a neural network  $q(z|x)$  is learned as a variational approximation to the conditional distribution  $P(Z|X)$ . The IM algorithm requires  $H(Z)$  and  $E_{XZ} \log q(z|x)$  to be tractable, which applies to latent codes of Variational Autoencoders (VAEs) and Generative Adversarial Networks (GANs) as well as categorical variables. [5] introduces mutual information lower bounds *MINE* and *MINE-f* which allow the modeling of general random variables and shows improved accuracy for high-dimensional random variables, with application to improving generative models. But as the high-capacity neural networks tend to overfit, *MINE* expects an impractically large number of samples to reach high confidence. [39] introduces a family of energy-based MI estimators with alternative forms of *MINE* and *MINE-f* lower bounds and provides new insights on bias-variance tradeoff of mutual information estimators [34]. [39] also introduces a new TCPC estimator with ongoing theoretical analysis.

Our work DEMINE introduces predictive mode and meta-learning to the *MINE* estimator family. By partitioning samples into training and validation to prevent overfitting, sample complexity is improved down to a practical level which enables statistical testing of dependency. Empirical bound tightness is improved by using meta-learning to learn more generalizable neural network models of the random variables.

**Meta-learning**, or "learning to learn", seeks to improve the generalization capability of neural networks by searching better hyper parameters [33], network architectures [38], initializations [11, 12, 30] and distance metrics [50, 46]. Meta-learning approaches has shown significant performance improvements in applications such as automatic neural architecture search [38], few-shot image recognition [11] and imitation learning [13].

In particular, our work is based on the Model-Agnostic Meta-Learning (MAML) [11] framework which is designed to improve few-shot learning performance. A network initialization is learned to maximize its performance when fine-tuned on few-shot learning tasks. Applications include few-shot image classification and navigation.

We leverage the model-agnostic nature of MAML for mutual information estimation between generic random variables. We adopt MAML for maximizing mutual information lower bounds. To construct a

collection of diverse tasks for MAML learning from limited samples, inspired by mutual information’s invariance to invertible transformations, we propose a task-augmentation protocol to automatically construct tasks by sampling random transformations to transform the samples. Results show reduced overfitting and better generalization.

### 3 Background

In this section<sup>2</sup>, we will provide the background necessary to understand our approach. We define  $X$  and  $Z$  to be two random variables,  $P(X, Z)$  is the joint distribution, and  $P(X)$  and  $P(Z)$  are the marginal distributions over  $X$  and  $Z$  respectively. Our goal is to estimate MI,  $I(X; Z)$  given *i.i.d.* sample pairs  $(x_i, z_i)$ ,  $i = 1, 2 \dots n$  from  $P(X, Z)$ . Let  $\mathcal{F} = \{T_\theta(x, z)\}_{\theta \in \Theta}$  be a class of scalar functions, where  $\theta$  is the set of model parameters. Let  $q(x|z) = p(x) \frac{e^{T_\theta(x, z)}}{\mathbb{E}_{(x, z) \sim P_{XZ}} e^{T_\theta(x, z)}}$ . the following energy-based family of lower bounds of MI hold for any  $\theta$ :

$$\begin{aligned} I(X; Z) &\geq \mathbb{E}_{(x, z) \sim P_{XZ}} \log \frac{q(x|z)}{p(x)} = \mathbb{E}_{(x, z) \sim P_{XZ}} T_\theta(x, z) - \mathbb{E}_{x \sim P_X} \log \mathbb{E}_{z \sim P_Z} e^{T_\theta(x, z)} \triangleq I_{\text{EB1}} [39] \\ &\geq \mathbb{E}_{(x, z) \sim P_{XZ}} T_\theta(x, z) - \log \mathbb{E}_{x \sim P_X, z \sim P_Z} e^{T_\theta(x, z)} \triangleq I_{\text{MINE}} [5] \\ &\geq \mathbb{E}_{(x, z) \sim P_{XZ}} T_\theta(x, z) - \mathbb{E}_{x \sim P_X, z \sim P_Z} e^{T_\theta(x, z)} + 1 \triangleq I_{\text{MINE-f}} [5], I_{\text{EB}} [39] \end{aligned} \quad (1)$$

where,  $\mathbb{E}$  is the expectation over the given distribution.

Based on  $I_{\text{MINE}}$ , the *MINE* estimator  $\widehat{I}(X; Z)_n$  is defined as in (2). Estimators for  $I_{\text{EB1}}$ ,  $I_{\text{MINE-f}}$  and  $I_{\text{EB}}$  can be defined similarly.

$$\widehat{I}(X; Z)_n = \sup_{\theta \in \Theta} \frac{1}{n} \sum_{i=1}^n T_\theta(x_i, z_i) - \log \frac{1}{n^2} \sum_{i=1}^n \sum_{j=1}^n e^{T_\theta(x_i, z_j)}. \quad (2)$$

With infinite samples to approximate expectation, (2) converges to the lower bound  $\widehat{I}(X; Z)_\infty$  specified in (3).

$$\widehat{I}(X; Z)_\infty = \sup_{\theta \in \Theta} I_{\text{MINE}} = \sup_{\theta \in \Theta} \mathbb{E}_{(X, Z) \sim P_{XZ}} T_\theta(X, Z) - \log \mathbb{E}_{X \sim P_X, Z \sim P_Z} e^{T_\theta(X, Z)}. \quad (3)$$

Note that the number of samples  $n$  needs to be substantially more than the number of model parameters  $d = |\theta|$  to prevent  $T_\theta(X, Y)$  from overfitting to the samples  $(x_i, z_i)$ ,  $i = 1, 2 \dots n$  and overestimating MI. Formally, the sample complexity of *MINE* is defined as the minimum number of samples  $n$  in order to achieve (4),

$$\Pr(|\widehat{I}(X, Z)_n - \widehat{I}(X, Z)_\infty| \leq \epsilon) \geq 1 - \delta. \quad (4)$$

Specifically, *MINE* proves that given the following assumptions:

1.  $T_\theta(X, Z)$  is  $L$ -Lipschitz,
2.  $T_\theta(X, Z) \in [-M, M]$ ,
3.  $\{\theta_i \in [-K, K], \forall i \in 1, \dots, d\}$ ,

making the minimum number of samples,  $n$ , to satisfy (4) to be (5).

$$n \geq \frac{2M^2(d \log(16KL\sqrt{d}/\epsilon) + 2dM + \log(2/\delta))}{\epsilon^2}. \quad (5)$$

For example, a neural network with dimension  $d = 10,000$ ,  $M = 1$ ,  $K = 0.1$  and  $L = 1$ , achieving a confidence interval of  $\epsilon = 0.1$  with 95% confidence would require  $n \geq 18,756,256$  samples. This is achievable for synthetic examples, *e.g.* the case illustrated in *MINE*, where  $X$  and  $Z$  are images and features generated by Generative Adversarial Networks (GANs). For real data, however, the cost of data acquisition for reaching statistically significant estimation can be prohibitively expensive.

We propose to use the MI lower bounds specified in Eq.1 from a prediction perspective, inspired by cross-validation. Our estimator, DEMINE, disentangles the data required for estimating the lower bound (which affects the sample complexity) from data for learning a generalizable  $T_\theta(X, Z)$  (which affects bound tightness). In DEMINE, the sample complexity is independent of model size, which enables high-confidence mutual information estimation on small datasets. Bound tightness is further improved by meta-learning which learns  $T_\theta(X, Z)$  for generalization.

<sup>2</sup>We are following the same notation as in [5].

## 4 Approach

In this section we formulate our approach. §4.1 specifies our estimator and two approaches on how to estimate MI using DEMINE and Meta-DEMINE using meta-learning; §4.2 derive the confidence interval of DEMINE which applies to both DEMINE and Meta-DEMINE; §4.3 further formulates the Meta-DEMINE approach, explains task augmentation and defines the optimization algorithms used for Meta-DEMINE.

### 4.1 Predictive Mutual Information Estimation

In DEMINE, we interpret the estimation of *MINE-f* lower bound<sup>3</sup> (1) as a learning problem. The goal is to infer the optimal network  $T_{\theta^*}(X, Z)$  with parameters  $\theta^*$  using a limited number of samples defined as follows:

$$\theta^* = \arg \max_{\theta \in \Theta} \mathbb{E}_{P_{XZ}} T_\theta(X, Z) - \mathbb{E}_{P_X} \mathbb{E}_{P_Z} e^{T_\theta(X, Z)} + 1$$

Specifically, samples from  $P(X, Z)$  are subdivided into a training set  $\{(x_i, z_i)_{\text{train}}, i = 1, \dots, m\}$  and a validation set  $\{(x_i, z_i)_{\text{val}}, i = 1, \dots, n\}$ . The training set is used for learning a network  $\tilde{\theta}$  as an approximation to  $\theta^*$  whereas the validation set is used for computing the DEMINE estimation  $\widehat{I}(X, Z)_{n, \tilde{\theta}}$  defined as in (6).

$$\widehat{I}(X, Z)_{n, \tilde{\theta}} = \frac{1}{n} \sum_{i=1}^n T_{\tilde{\theta}}(x_i, z_i)_{\text{val}} - \frac{1}{n^2} \sum_{i=1}^n \sum_{j=1}^n e^{T_{\tilde{\theta}}(x_i, z_j)_{\text{val}}} + 1 \quad (6)$$

We propose two approaches to learn  $\tilde{\theta}$ , DEMINE, specified in this section and Meta-DEMINE in §4.3.

**DEMINE** learns  $\tilde{\theta}$  by maximizing the mutual information lower bound on the training set (fitting the training set) as follows:

$$\begin{aligned} \tilde{\theta} &= \arg \min_{\theta \in \Theta} \mathcal{L}(\{(x, z)\}_{\text{val}}, \theta), \text{ where,} \\ \mathcal{L}(\{(x, z)\}_{\mathcal{B}}, \theta) &= -\frac{1}{|\mathcal{B}|} \sum_{i=1}^{|\mathcal{B}|} T_\theta(x_i, z_i)_{\mathcal{B}} + \frac{1}{|\mathcal{B}|^2} \sum_{i=1}^{|\mathcal{B}|} \sum_{j=1}^{|\mathcal{B}|} e^{T_\theta(x_i, z_j)_{\mathcal{B}}} - 1. \end{aligned} \quad (7)$$

DEMINE algorithm is illustrated in Algorithm 1.

### 4.2 Sample complexity analysis

Since  $\tilde{\theta}$  is learned independently of validation samples  $\{(x_i, z_i)_{\text{val}}, i = 1, \dots, n\}$ , the sample complexity of the DEMINE estimator,  $\widehat{I}(X, Z)_{n, \tilde{\theta}}$ , does not involve the model class  $\mathcal{F}$  and the sample complexity is greatly reduced compared to *MINE-f*. DEMINE estimates  $\widehat{I}(X, Z)_{\infty, \tilde{\theta}}$  defined as:

$$\widehat{I}(X, Z)_{\infty, \tilde{\theta}} = \mathbb{E}_{P_{XZ}} T_{\tilde{\theta}}(X, Z) - \mathbb{E}_{P_X} \mathbb{E}_{P_Z} e^{T_{\tilde{\theta}}(X, Z)} + 1$$

when infinite number of samples are provided. As shown in (8),  $\widehat{I}(X, Z)_{\infty, \tilde{\theta}}$  lower bounds mutual information.

$$\begin{aligned} \widehat{I}(X, Z)_{\infty, \tilde{\theta}} &= \mathbb{E}_{P_{XZ}} T_{\tilde{\theta}}(X, Z) - \mathbb{E}_{P_X} \mathbb{E}_{P_Z} e^{T_{\tilde{\theta}}(X, Z)} + 1 \\ &\leq \sup_{\theta \in \Theta} \mathbb{E}_{P_{XZ}} T_\theta(X, Z) - \mathbb{E}_{P_X} \mathbb{E}_{P_Z} e^{T_\theta(X, Z)} + 1 \\ &\leq I(X; Z) \end{aligned} \quad (8)$$

We now derive the sample complexity of DEMINE defined as the number of samples  $n$  required for

<sup>3</sup>The *MINE* lower bound (1) can be interpreted in the same way, but will result in a higher sample complexity than the *MINE-f* lower bound. In this work, we choose to focus on *MINE-f* in favor of a lower sample complexity over bound tightness.

---

**Algorithm 1** DEMINE

---

**Input Data:**  $\{(x, z)_{\text{train}}, (x, z)_{\text{val}}\}$   
**Parameters:** Batch  $\mathcal{B}$ , Iterations  $N$ , Learning rate  $\eta$   
**Output:** MI,  $T_{\theta}(X, Z)$

- 1:  $\theta^{(0)} \leftarrow$  Xavier Initialization [19]
- 2: **for**  $i = 1 : N$  **do**
- 3:     Sample a batch of  $(x_i, z_i)_{\mathcal{B}} \sim (x, z)_{\text{train}}$
- 4:     Compute  $\mathcal{L}((x_i, z_i)_{\mathcal{B}}, \theta^{(i-1)})$  using (7)
- 5:     Compute  $\nabla_{\theta}^{(i)} \mathcal{L}$  – gradient for  $\theta$
- 6:     Update  $\theta^{(i)}$  using Adam Optimizer [31] with  $\eta$
- 7: **end for**
- 8: MI =  $\widehat{I}(X, Z)_{n, \theta^{(N)}}$  using (6)
- 9: **return** MI,  $\theta^{(N)}$

---

$\widehat{I}(X, Z)_{n, \tilde{\theta}}$  to be a good approximation to  $\widehat{I}(X, Z)_{\infty, \tilde{\theta}}$  in Theorem 1.

**Theorem 1.** For  $T_{\tilde{\theta}}(X, Z)$  bounded by  $[L, U]$ , given any accuracy  $\epsilon$  and confidence  $\delta$ , we have:

$$\Pr(|\widehat{I}(X, Z)_{n, \tilde{\theta}} - \widehat{I}(X, Z)_{\infty, \tilde{\theta}}| \leq \epsilon) \geq 1 - \delta$$

when the number of validation samples  $n$  satisfies:

$$n \geq n^*, \text{ where } \min_{0 \leq \xi \leq \epsilon} 2e^{-\frac{2\xi^2 n^*}{(U-L)^2}} + 4e^{-\frac{(\epsilon-\xi)^2 n^*}{2(e^U-e^L)^2}} = \delta \quad (9)$$

**Proof.** Since  $T_{\tilde{\theta}}(X, Z)$  is bounded by  $[L, U]$ , applying the Hoeffding inequality to the first half of Eq. 6 gives us:

$$\Pr\left(\left|\frac{1}{n} \sum_{i=1}^n T_{\tilde{\theta}}(x_i, z_i) - \mathbb{E}_{P_{XZ}} T_{\tilde{\theta}}(X, Z)\right| \geq \xi\right) \leq 2e^{-\frac{2\xi^2 n}{(U-L)^2}}$$

Similarly, as  $e^{T_{\theta}(X, Z)}$  is bounded by  $[e^L, e^U]$ , applying the Hoeffding inequality to the second half, we have:

$$\begin{aligned} \Pr\left(|\mathbb{E}_{P_X} \mathbb{E}_{P_Z} e^{T_{\theta}(X, Z)} - \frac{1}{n} \sum_{i=1}^n \mathbb{E}_{P_Z} e^{T_{\tilde{\theta}}(x_i, z)}| \geq \zeta\right) &\leq 2e^{-\frac{2\xi^2 n}{(e^U-e^L)^2}} \\ \Pr\left(|\mathbb{E}_{P_Z} \frac{1}{n} \sum_{i=1}^n e^{T_{\theta}(x_i, z)} - \frac{1}{n} \sum_{j=1}^n \frac{1}{n} \sum_{i=1}^n e^{T_{\tilde{\theta}}(x_i, z_j)}| \geq \zeta\right) &\leq 2e^{-\frac{2\xi^2 n}{(e^U-e^L)^2}}. \end{aligned}$$

Combining the above bounds gives

$$\Pr(|\widehat{I}(X, Z)_{n, \tilde{\theta}} - \widehat{I}(X, Z)_{\infty, \tilde{\theta}}| \leq \xi + 2\zeta) \geq 1 - 2e^{-\frac{2\xi^2 n}{(U-L)^2}} - 4e^{-\frac{2\xi^2 n}{(e^U-e^L)^2}}$$

By solving  $\xi$  to minimize  $n$  according to (9), we have,

$$\Pr(|\widehat{I}(X, Z)_{n, \tilde{\theta}} - \widehat{I}(X, Z)_{\infty, \tilde{\theta}}| \leq \epsilon) \geq 1 - \delta. \quad \blacksquare$$

Compared to *MINE*, as per the example shown in §3, for  $M = 1$  (i.e.  $L = -1$  and  $U = 1$ ),  $\delta = 0.05$ ,  $\epsilon = 0.1$ , our estimator requires only  $n = 4,495$  compared to *MINE* requiring  $n = 18,756,256$  i.i.d validation samples to estimate a lower bound, which makes mutual information-based dependency analysis feasible for domains where data collection is prohibitively expensive, e.g. fMRI brain scans. In practice, sample complexity can be further optimized by tuning hyper-parameters  $U$  and  $L$ .

Note that the sample complexity of our approach, DEMINE, for estimating (8) does not depend on network size  $d$ . The improved sample complexity seemingly comes at a cost of bound tightness guarantees. In fact, to guarantee bound tightness of (8),  $O(d \log d)$  examples would still be theoretically required to learn  $\tilde{\theta}$  with guaranteed close values to  $\theta^*$ , and the total data cost would

---

**Algorithm 2** Meta-DEMINE

---

**Input Data:**  $\{(x, z)_{\text{train}}, (x, z)_{\text{val}}\}$   
**Parameters:** batch  $\mathcal{B}$ , Meta Learning Iterations  $N_M$ , Task Augmentation Iterations  $N_T$ , Optimization Iterations  $N_O$ , Ratio  $r$ , Learning rate  $\eta$ , Meta Learning Rate  $\eta_{\text{meta}}$   
**Output:** MI,  $T_{\theta_{\text{init}}}(X, Z)$ ,  $T_{\theta}(X, Z)$

```

1: for  $i = 1 : N_M$  do
2:   for  $j = 1 : N_T$  do
3:      $A = r \times \text{train}$ ,  $B = \text{train} - A$ 
4:     Split  $(x, z)_{\text{train}}$  into  $(x, z)_A$  and  $(x, z)_B$ 
5:     Transformation  $R_x$  for  $x$ ,  $R_x(\cdot) = P(G(O(\cdot)))$ 
6:     Transformation  $R_z$  for  $z$ ,  $R_z(\cdot) = P(G(O(\cdot)))$ 
7:      $\theta_{\text{meta}}^{(0)} \leftarrow \theta_{\text{init}}$ 
8:     for  $k = 1 : N_O$  do
9:       Sample a batch of  $(x, z)_B \sim (x, z)_A$ 
10:      Compute  $\mathcal{L}((R_x(x), R_z(z))_B, \theta_{\text{meta}}^{(k)})$  using (7)
11:      Compute  $\nabla_{\theta_{\text{meta}}^{(k)}} \mathcal{L}$  – gradient for  $\theta_{\text{meta}}$ 
12:      Update  $\theta_{\text{meta}}$  using Vanilla SGD4 with  $\eta$ 
13:    end for
14:    Compute  $\mathcal{L}_{\text{meta}}((R_x(x), R_z(z))_B, \theta_{\text{meta}}^{(N_O)})$  using (7)
15:    Compute  $\nabla_{\theta_0} \mathcal{L}_{\text{meta}}$  – gradient to  $\theta_{\text{init}}$  using BPTT
16:  end for
17:  Update  $\theta_{\text{init}}$  using Adam [31] with  $\eta_{\text{meta}}$ 
18: end for
19:  $\theta^{(0)} \leftarrow \theta_{\text{init}}$ 
20: for  $i = 1 : N_O$  do
21:   Sample a batch of  $(x, z)_B \sim (x, z)_{\text{train}}$ 
22:   Compute  $\mathcal{L}((x, z)_B, \theta^{(i)})$  using (7)
23:   Compute gradient  $\nabla_{\theta} \mathcal{L}$ 
24:   Update  $\theta$  using Adam with  $\eta$ 
25: end for
26: Compute MI =  $\mathcal{L}((x, z)_{\text{val}}, \theta^{(N_O)})$ 
27: return MI,  $\theta_{\text{init}}$ ,  $\theta^{(N_O)}$ 

```

---

be on par with *MINE*. In practice, however, such a learnability bound is known to be overly loose, as over-parameterized neural networks have been shown to generalize well in classification and regression tasks.

Fundamentally, what determines bound tightness is the generalization error of  $\tilde{\theta}$  – to which the learnability bound is serving as a proxy. Empirically, not only that the bound tightness of DEMINE is as good as *MINE* so the loss of guaranteed tightness did not affect empirical tightness, but the learning-based formulation of DEMINE also allows further bound tightness improvements by learning  $\tilde{\theta}$  that generalizes beyond curve fitting using meta learning. In the following section, we present a meta learning formulation, Meta-DEMINE, that learns  $\tilde{\theta}$  for generalization given the same model class and training samples.

### 4.3 Meta Learning

Given training data  $\{(x_i, z_i)_{\text{train}}, i = 1, \dots, m\}$ , Meta-DEMINE algorithm first generates mutual information estimation tasks each consisting of a meta-training split A and a meta-val split B through a novel *task augmentation* process. A parameter initialization  $\theta_{\text{init}}$  is then learned to maximize mutual information estimation performance on the generated tasks using initialization  $\theta_{\text{init}}$  as shown in (10).

$$\begin{aligned}
\theta_{\text{init}} &= \arg \min_{\theta^{(0)} \in \Theta} \mathbb{E}_{(A, B) \in \mathcal{T}} \mathcal{L}((x, z)_B, \theta^{(t)}), \\
\text{with,} \\
\theta^{(t)} &\equiv \text{MetaTrain}((x, z)_A, \theta^{(0)}).
\end{aligned} \tag{10}$$

Here  $\theta^{(t)} = \text{MetaTrain}((x, z)_A, \theta^{(0)})$  is the meta-training process of starting from an initialization  $\theta^{(0)}$  and applying SGD over  $t$  steps to learn  $\theta$  where in every meta training iteration we have:

$$\theta^{(t)} \leftarrow \theta^{(t-1)} - \gamma \nabla \mathcal{L}((x, z)_A, \theta^{(t-1)}).$$

Finally,  $\tilde{\theta}$  is learned using the entire training set  $\{(x_i, z_i)_{\text{train}}, i = 1, \dots, m\}$  with  $\theta_{\text{init}}$  as the initialization as follows:

$$\tilde{\theta} = \text{MetaTrain}((x, z)_{\text{train}}, \theta_{\text{init}}).$$

**Task Augmentation:** Meta-DEMINE adapts Model-Agnostic Meta-Learning (MAML) [11] for mutual information lower bound maximization. MAML has been shown to improve generalization performance in  $N$ -class  $K$ -shot image classification. Mutual information estimation, however, does not come with predefined classes and tasks. A naive approach to produce tasks would be through cross validation – partitioning training data into meta-training and meta-validation splits. However, merely using cross-validation tasks is prone to overfitting – a  $\theta_{\text{init}}$ , which memorizes all training samples would as a result have memorized all meta-validation splits.

Instead, Meta-DEMINE generates tasks by augmenting the cross validation tasks through *task augmentation*. Training samples are first split into meta-training and meta-validation splits, and then transformed using the same random invertible transformation to increase task diversity. Meta-DEMINE generates invertible transformation by sequentially composing the following functions:

$$\begin{aligned} \text{Offset} : \quad O(x) &= x + \epsilon, & \epsilon &\sim \mathcal{U}(-0.1, 0.1), \\ \text{Gamma} : \quad G(x) &= \text{sign}(x) |x|^\gamma, & \gamma &\sim \mathcal{U}(0.5, 2), \\ \text{Permute} : \quad P(x) &= {}^n P_d, & &\text{Permute dimensions.} \end{aligned}$$

Since the mutual information between two random variables is invariant to invertible transformations on each of variables, MetaTrain is expected to arrive at the same mutual information lower bound estimation regardless of the transformation applied. At the same time, memorization is greatly suppressed, as the same pair  $(x, z)$  can have different  $P(x, z)$  under different transformations. More sophisticated invertible transformations (affine, piece-wise linear) can be added with ease.

Task augmentation is an orthogonal approach to data augmentation. Using image classification as an example, data augmentation generates variations of the image, translated, or rotated images assuming that they are valid examples of the class. Task augmentation on the other hand, does not make such assumption. Task augmentation requires the initial parameters  $\theta_{\text{init}}$  to be capable of recognizing the same class in a world where all images are translated and/or rotated, with the assumption that the optimal initialization should easily adapt to both the upright world and the translated and/or rotated world.

**Optimization:** Solving  $\theta_{\text{init}}$  using the meta learning formulation (10) poses a challenging optimization problem. Computing gradient for  $\theta_{\text{init}}$  requires back-propagating the model training process  $\text{MetaTrain}((x, z)_A, \theta^{(0)})$ . One approach to compute gradient for  $\theta_{\text{init}}$  is using back propagation through time (BPTT) which is used in MAML. It back propagates through the optimization process  $\text{MetaTrain}((x, z)_A, \theta^{(0)})$  using second order gradients. BPTT is an effective approach for a small number of optimization steps, but is vulnerable to exploding and vanishing gradients. In addition to BPTT, we find stochastic finite difference algorithms such as Evolution Strategies (ES) [41] and Parameter-Exploring Policy Gradients (PEPG) [43] effective for solving (10). They generally produce noisy yet robust gradient estimates. In addition, they are memory efficient and allow the use of complex optimizers such as Adam [31] in  $\text{MetaTrain}((x, z)_A, \theta^{(0)})$ . In practice, we use BPTT or PEPG to optimize (10) depending on the problem.

Meta-DEMINE algorithm is described in Algorithm 2.

## 5 Synthetic Evaluations

In this section, we evaluate our approaches DEMINE and Meta-DEMINE against baselines and state-of-the-art approaches on synthetic datasets. First, in §5.1, we describe the different datasets. Then, in §5.2, we specify the approaches evaluated. Finally, in §5.3 we present our experiments results.

### 5.1 Synthetic Datasets

**Multivariate Gaussian:** Following [5], we define two  $k$ -dimensional multivariate Gaussian random variables  $X$  and  $Z$  which have component-wise correlation  $\text{corr}(X_i, Z_j) = \delta_{ij}\rho$ , where  $\rho \in (-1, 1)$  and  $\delta_{ij}$  is Kronecker's delta. Mutual information  $I(X; Z)$  has a closed form solution  $I(X; Z) = -k \ln(1 - \rho^2)$ . We vary the parameter  $\rho \in \{0, 0.1, 0.3, 0.5, 0.7\}$  and  $\rho \in \{0.05, 0.1, 0.15, 0.2, 0.25\}$

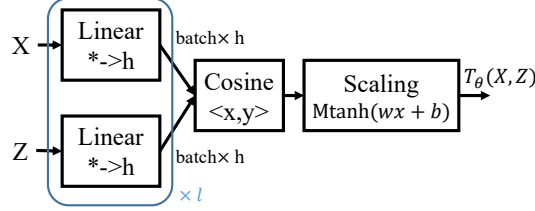


Figure 1: Network architecture used for synthetic experiments. Incoming samples of random variables  $X$  and  $Z$  are encoded using MLP and are combined using cosine distance followed by a scaling layer.

for  $k = 1$  and  $k = 10$  respectively. We also vary number of samples  $n \in \{200, 600, 2000, 6000\}$ . For each setting, we generate 10 datasets using 10 different random seeds.

**Noisy sine wave regression:** We define two random variables  $X$  and  $Z$ , where  $Z = \sin(aX) + 0.05\epsilon$ ,  $X \sim \mathcal{U}(-1, 1)$  and  $\epsilon \sim \mathcal{N}(0, 1)$ . Estimating mutual information accurately given few pairs of  $(X, Z)$  requires the ability to extrapolate the sine wave given few examples. We vary the parameter  $a \in \{20, 30\}$  to generate sine waves of different frequencies. We also vary the number of samples  $n \in \{800, 2000\}$ . As a closed-form mutual information solution does not exist, we run the MI-Kraskov [32] mutual information estimator on 1,000,000 samples drawn from the sine wave as an estimation of ground truth. Same as multivariate Gaussian, we generate 10 datasets for each setting using 10 random seeds.

## 5.2 Experiment Setup

In our experiments we compare the following approaches:

**DEMINE:** Our base algorithm for estimating mutual information lower bound introduced in §4.1. We split the samples  $(x, z)$  into 50%-50% as  $(x, z)_{\text{train}}$  and  $(x, z)_{\text{val}}$ . We use a multi-layer perceptron (MLP) network with cosine distance on top for  $T_\theta(X, Z)$  shown in Figure. 1.  $X$  and  $Z$  are each encoded using an MLP into embeddings. Cosine similarity is used to join the embeddings, followed by a scaling function  $M \tanh(wx + b)$  to control the bound in  $[-M, M]$ , where we fix  $M = 3$ . We select the MLP hyper-parameters – hidden size  $h \in \{32, 64, 256\}$  and number of layers  $\in \{2, 3, 4\}$ , learning rate  $l\eta \in \{10^{-4}, 3 \times 10^{-4}, 10^{-3}, 3 \times 10^{-3}, 10^{-2}, 3 \times 10^{-2}, 10^{-1}\}$  and number of iterations  $N \in \{5, 10, 20, 50, 100, 200, 500, 1000, 2000\}$  – through a grid search using 4-fold cross-validation on  $(x, z)_{\text{train}}$ .

**Meta-DEMINE:** Our meta learning algorithm for estimating mutual information lower bound introduced in §4.3. We use the same 50%-50% split of the data into  $(x, z)_{\text{train}}$  and  $(x, z)_{\text{val}}$ . The model architecture and hyper parameters as specified in DEMINE, with additional optimization-related hyper parameters fixed to  $N_M = 5,000$ ,  $N_T = 3$ ,  $\eta_{\text{meta}} = 3 \times 10^{-3}$ , ratio  $r = 0.8$  for faster optimization. PEPG [43] is used for computing gradient for meta-optimization due to the large  $N_O$ .

**MINE-f-ES<sup>5</sup>:** *Mine-f* with early stopping, the *MINE* mutual information lower bound estimator [5] introduced in §3, but augmented with early stopping to reduce overfitting. We use *MINE-f* and stop optimization before  $T_\theta(X, Z)$  overfits, by selecting hyperparameters using the same cross validation protocol as DEMINE, and compute *MINE-f-ES*. *MINE-f* with early stopping receives the entire set of samples  $(x, z)$  and use the same model architecture as DEMINE.

**MI-Kraskov:** The KSG estimator [32], a  $k$ -NN-based non-parametric mutual information estimator. We use publicly available implementations<sup>6</sup>, which computes mutual information between high-dimensional random variable  $X$  and one-dimensional random variable  $Z$ . We use the entire set of samples  $(x, z)$  and the default hyper parameter `n_neighbors = 3`.

<sup>5</sup>As we focus on mutual information estimation performance using few samples, optimizing *MINE* to convergence will result in overfitting and *MINE* will almost always incorrectly report  $\widehat{I}(X, Z)_n = M$  which will not make a meaningful comparison.

<sup>6</sup>Scikit-learn for 1-D random variables: [https://scikit-learn.org/stable/modules/generated/sklearn.feature\\_selection.mutual\\_info\\_classif.html](https://scikit-learn.org/stable/modules/generated/sklearn.feature_selection.mutual_info_classif.html) where estimator outputs are thresholded to be non-negative. Implementation by [17] for high-dimensional random variables <https://github.com/wgao9/knrie>.

### 5.3 Result

Mutual estimation results for all the 1-Dimensional (1D) Gaussian, 10-dimensional (10D) Gaussian and sine wave datasets are available in Figure 2, 3 and 4 respectively. For each dataset we run each algorithm on datasets generated using 10 different seeds. We report 95% confidence intervals of DEMINE and Meta-DEMINE lower bound based on (4). We report confidence intervals of *MINE-f-ES* lower bound based on (5), in which  $d$  and  $K$  are computed from  $\theta$  while assuming  $L = 1$ . MI-Kraskov mutual information estimator, however, does not come with analytical bound guarantees. The numerical values of the mean values over 10 runs and the confidence intervals are reported in Tables 1, 2 and 3.

**The 1D Gaussian results:** results in Figure 2 serves as a consistency check. Both DEMINE and Meta-DEMINE are able to reliably estimate mutual information bounds for all  $\rho$ s given  $n \geq 300$  samples. Notably, for 1D Gaussian  $\rho = 0.0$  (Figure 2 first row), MI-Kraskov and *MINE-f-ES* both constantly predict positive values yet the true mutual information is 0, even at 1,000 samples when 1,000 points have been sampled between  $X \in \mathcal{U}(-1, 1)$ . We find that in general, *MINE-f-ES* and MI-Kraskov tend to produce aggressive mutual information estimates, which often seems to be closer to the true mutual information values, yet are not justified and with extremely loose confidence intervals. Given a positive detection yet with a low confidence, it would be impossible to conclude if  $X$  and  $Z$  are statistically dependent or not. DEMINE and Meta-DEMINE produce lower bound estimations with tighter confidence intervals. For 1D Gaussian  $\rho = 0.0$ , lower bound estimations by DEMINE and Meta-DEMINE are mostly negative, with 95% confidence intervals consistent with the null hypothesis  $I(X; Z) = 0$ . For 1D Gaussian  $\rho = 0.5$  (Figure 2 fifth row)  $n = 2000$ , DEMINE and Meta-DEMINE signals statistically significant dependency.

**The 10D Gaussian results:** results in Figure 3 tests the performance of MI estimation for high-dimensional random variables. The gap between the estimations and the ground truth MI becomes visibly larger than the 1D Gaussian case, which demonstrates the challenge of MI estimation with few samples in high-dimensional space. *MINE-f-ES* produces lower bound estimations closest to the ground truth MI yet are low confidence and overshoot on few samples. DEMINE provides high-confidence estimations close to the ground truth, and Meta-DEMINE slightly but consistently improves the estimations of DEMINE. MI-Kraskov on the other hand, provides estimations far from ground truth.

**Sine wave results:** The effect of meta learning is most significant for sine wave result shown in Figure 4. Despite delivering good performance for 1D Gaussians, MI-Kraskov significantly under estimates the amount of mutual information available in the 1D sine waves. DEMINE detects significant dependency in the 2000 sample cases. By incorporating MAML which have been shown to learn the structure of sine waves, Meta-DEMINE significantly improves mutual information estimation results and are even able to detect significant dependency in the  $a = 20$  400 samples case.

To study the effect of task augmentation, we compare the performance of Meta-DEMINE with and without task augmentation for 10D Gaussian  $\rho = 0.2$  using 6000 samples. Figure 5 shows the progression of the MI estimation (left) as well as the inverse trainloss (right) over the course of training. Indeed, maximizing cross-validation performance without task augmentation results in rapid overfitting and very little performance gain. With task augmentation on, the inverse trainloss reduces due to the difficulty of performing all the augmented tasks. The MI estimation, however, shows no overfitting in 2500 iterations with performance keep increasing to beyond DEMINE through the course of training.

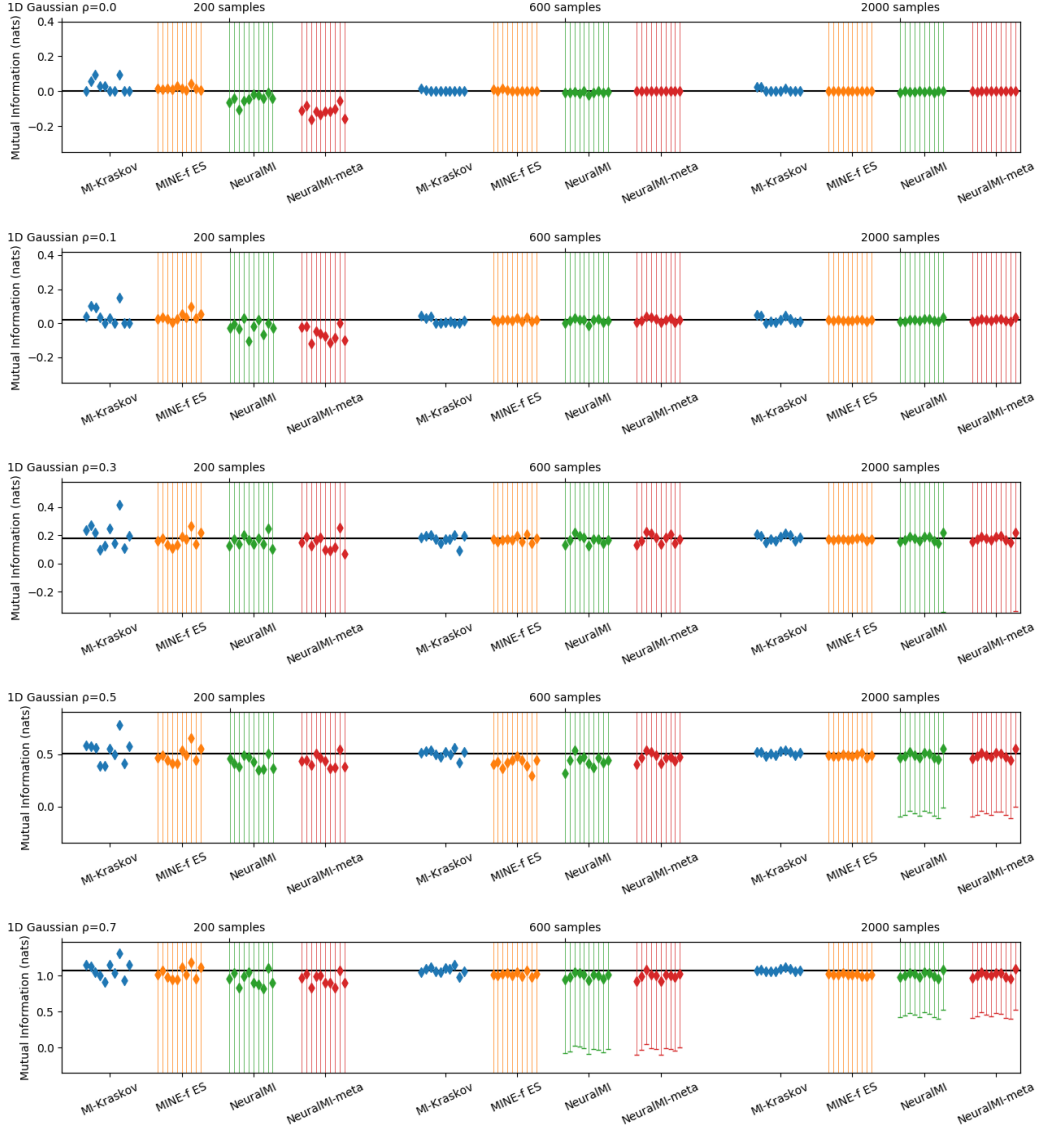


Figure 2: 1D Gaussian results for MI-Kraskov, *MINE-f* with early stopping (MINE-f ES), DEMINE and Meta-DEMINE on 1D correlated Gaussian random variables with correlation  $\rho \in \{0.0, 0.1, 0.3, 0.5, 0.7\}$  (top to bottom) and number of samples  $n \in \{200, 600, 2000\}$  (left to right). Results of 10 runs with confidence intervals are recorded and visualized. Ground truth MI is visualized as the horizontal line. MI-Kraskov and MINE-f ES makes aggressive yet low confidence estimations which can be seen in the  $\rho = 0.0$  case. DEMINE and Meta-DEMINE detects statistically significant dependency for  $\rho = 0.5$  and  $\rho = 0.7$ .

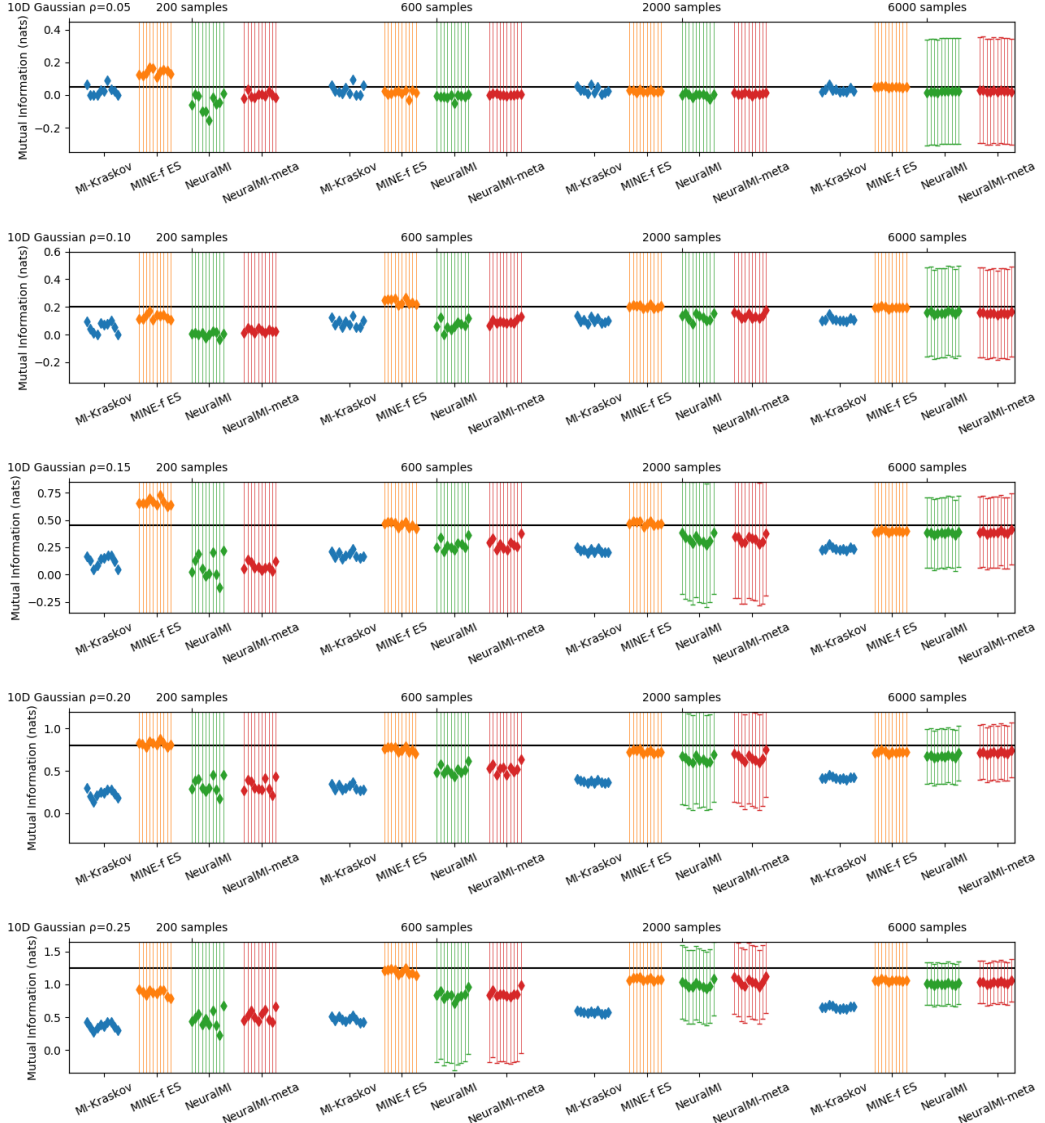


Figure 3: 10D Gaussian results for MI-Kraskov, MINE- $f$  with early stopping (MINE- $f$  ES), DEMINE and Meta-DEMINE on 10D diagonally correlated Gaussian random variables with correlation  $\rho \in \{0.05, 0.10, 0.15, 0.20, 0.25\}$  (top to bottom) and number of samples  $n \in \{200, 600, 2000, 6000\}$  (left to right). Results of 10 runs with confidence intervals are recorded and visualized. Ground truth MI is visualized as the horizontal line. MINE- $f$  ES makes aggressive yet low confidence estimations which can be seen in the  $\rho = 0.05$  case. MI-Kraskov under estimates mutual information. DEMINE and Meta-DEMINE detects statistically significant dependency for  $\rho = 0.15, 0.20, 0.25$ .

Table 1: Mean and confidence intervals for 1D Gaussian. Statistically significant dependency is marked in bold font.

Approach	1D Gaussian $\rho = 0.0$				1D Gaussian $\rho = 0.1$			
	200	600	2000		200	600	2000	
MI-Kraskov	0.031	0.003	0.007		0.044	0.014	0.021	
<i>MINE-f</i> ES	$0.017 \pm 60.109$	$0.005 \pm 298.833$	$0.001 \pm 19.008$		$0.038 \pm 151.356$	$0.019 \pm 49.591$	$0.017 \pm 13.396$	
DEMINE	$-0.044 \pm 1.776$	$-0.008 \pm 1.026$	$-0.003 \pm 0.562$		$-0.023 \pm 1.776$	$0.014 \pm 1.026$	$0.018 \pm 0.562$	
Meta-DEMINE	$-0.115 \pm 1.776$	$-0.000 \pm 1.026$	$-0.000 \pm 0.562$		$-0.064 \pm 1.776$	$0.021 \pm 1.026$	$0.019 \pm 0.562$	
Ground Truth	0.000				0.020			
Approach	1D Gaussian $\rho = 0.3$				1D Gaussian $\rho = 0.5$			
	200	600	2000		200	600	2000	
MI-Kraskov	0.207	0.174	0.183		0.533	0.510	0.513	
<i>MINE-f</i> ES	$0.171 \pm 42.363$	$0.172 \pm 42.738$	$0.172 \pm 13.396$		$0.492 \pm 517.595$	$0.413 \pm 49.591$	$0.492 \pm 38.790$	
DEMINE	$0.161 \pm 1.776$	$0.168 \pm 1.026$	$0.175 \pm 0.562$		$0.423 \pm 1.776$	$0.435 \pm 1.026$	$0.493 \pm 0.562$	
Meta-DEMINE	$0.144 \pm 1.776$	$0.176 \pm 1.026$	$0.179 \pm 0.562$		$0.436 \pm 1.776$	$0.470 \pm 1.026$	$0.494 \pm 0.562$	
Ground Truth	0.180				0.511			
Approach	1D Gaussian $\rho = 0.7$							
	200	600	2000					
MI-Kraskov	1.080	1.077	1.078					
<i>MINE-f</i> ES	$1.035 \pm 42.363$	$1.020 \pm 42.738$	$1.015 \pm 114.176$					
DEMINE	$0.947 \pm 1.776$	$0.994 \pm 1.026$	<b>1.015 <math>\pm 0.562</math></b>					
Meta-DEMINE	$0.944 \pm 1.776$	$0.997 \pm 1.026$	<b>1.014 <math>\pm 0.562</math></b>					
Ground Truth	1.072							

Table 2: Mean and confidence intervals for 10D Gaussian. Statistically significant dependency is marked in bold font.

Approach	10D Gaussian $\rho = 0.05$				10D Gaussian $\rho = 0.10$			
	200	600	2000	6000	200	600	2000	6000
MI-Kraskov	0.027	0.032	0.030	0.032	0.054	0.086	0.102	0.110
<i>MINE-f</i> ES	$0.140 \pm 122.666$	$0.014 \pm 42.738$	$0.024 \pm 38.790$	$0.049 \pm 10.974$	$0.130 \pm 85.894$	$0.240 \pm 208.455$	$0.202 \pm 27.162$	$0.197 \pm 22.396$
DEMINE	$-0.052 \pm 1.776$	$-0.010 \pm 1.026$	$-0.001 \pm 0.562$	$0.021 \pm 0.324$	$0.002 \pm 1.776$	$0.068 \pm 1.026$	$0.126 \pm 0.562$	$0.161 \pm 0.324$
Meta-DEMINE	$0.000 \pm 1.776$	$0.001 \pm 1.026$	$0.008 \pm 0.562$	$0.025 \pm 0.324$	$0.028 \pm 1.776$	$0.094 \pm 1.026$	$0.139 \pm 0.562$	$0.154 \pm 0.324$
Ground Truth	0.050				0.200			
Approach	10D Gaussian $\rho = 0.15$				10D Gaussian $\rho = 0.20$			
	200	600	2000	6000	200	600	2000	6000
MI-Kraskov	0.124	0.180	0.218	0.240	0.231	0.307	0.374	0.421
<i>MINE-f</i> ES	$0.661 \pm 85.894$	$0.457 \pm 208.455$	$0.470 \pm 13.396$	$0.399 \pm 7.734$	$0.822 \pm 85.894$	$0.754 \pm 24.458$	$0.728 \pm 13.396$	$0.724 \pm 7.734$
DEMINE	$0.070 \pm 1.776$	$0.271 \pm 1.026$	$0.326 \pm 0.562$	<b>0.381 <math>\pm 0.324</math></b>	$0.329 \pm 1.776$	$0.508 \pm 1.026$	<b>0.640 <math>\pm 0.562</math></b>	<b>0.675 <math>\pm 0.324</math></b>
Meta-DEMINE	$0.077 \pm 1.776$	$0.279 \pm 1.026$	$0.324 \pm 0.562$	<b>0.390 <math>\pm 0.324</math></b>	$0.326 \pm 1.776$	$0.528 \pm 1.026$	<b>0.659 <math>\pm 0.562</math></b>	<b>0.718 <math>\pm 0.324</math></b>
Ground Truth	0.450				0.800			
Approach	10D Gaussian $\rho = 0.25$							
	200	600	2000	6000				
MI-Kraskov	0.364	0.467	0.575	0.651				
<i>MINE-f</i> ES	$0.871 \pm 42.363$	$1.194 \pm 49.591$	$1.080 \pm 114.176$	$1.061 \pm 10.974$				
DEMINE	$0.460 \pm 1.776$	$0.835 \pm 1.026$	<b>0.996 <math>\pm 0.562</math></b>	<b>1.005 <math>\pm 0.324</math></b>				
Meta-DEMINE	$0.524 \pm 1.776$	$0.860 \pm 1.026$	<b>1.042 <math>\pm 0.562</math></b>	<b>1.029 <math>\pm 0.324</math></b>				
Ground Truth	1.252							

Table 3: Mean and confidence intervals for synthetic sine wave. Statistically significant dependency is marked in bold font.

Number of samples	Sine wave $a = 20$				Sine wave $a = 30$			
	800	2000		800	2000		800	2000
MI-Kraskov	0.935	1.528		0.592	1.020			
<i>MINE-f</i> ES	$1.690 \pm 258.797$	$1.811 \pm 202.122$		$0.937 \pm 319.583$	$1.530 \pm 163.678$			
DEMINE	<b>1.149 <math>\pm 0.888</math></b>	<b>1.582 <math>\pm 0.562</math></b>		$0.729 \pm 0.888$	<b>1.297 <math>\pm 0.562</math></b>			
Meta-DEMINE	<b>1.529 <math>\pm 0.888</math></b>	<b>1.793 <math>\pm 0.562</math></b>		<b>1.240 <math>\pm 0.888</math></b>	<b>1.426 <math>\pm 0.562</math></b>			
Ground Truth (est.)	2.304				2.299			

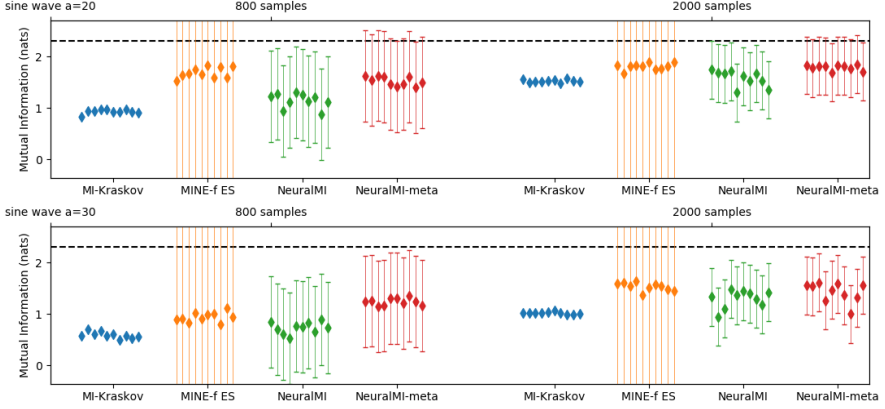


Figure 4: Sine wave results for MI-Kraskov, *MINE-f* with early stopping (MINE-f ES), DEMINE and Meta-DEMINE on 1D random variables ( $X, Y$ ) where  $Y = \sin(aX)$ .  $a \in \{20, 30\}$  (top to bottom) and number of samples  $n \in \{800, 2000\}$  (left to right). Results of 10 runs with confidence intervals are recorded and visualized. Estimated MI from 1,000,000 samples is visualized as the horizontal dashed line. MINE-f ES makes aggressive yet low confidence estimations. MI-Kraskov under estimates mutual information. DEMINE and Meta-DEMINE detects statistically significant dependency for both datasets. Meta-DEMINE shows significant accuracy improvements over DEMINE.

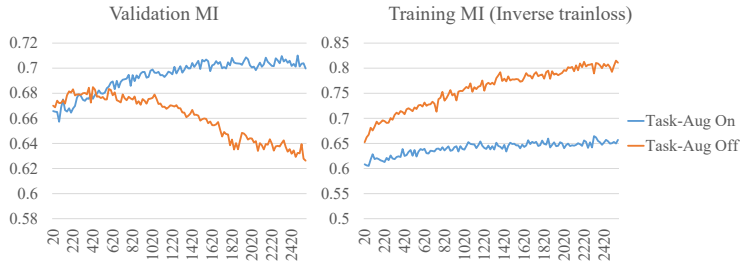


Figure 5: Validation MI estimation and trainloss progress of running Meta-DEMINE with and without task augmentation on 10D Gaussian  $\rho = 0.20$ ,  $n = 6000$  over 2500 iterations. Without task augmentation, Meta-DEMINE quickly overfits and shows only small improvements on top of DEMINE. Task augmentation reduces overfitting as well as greatly improves mutual information estimation results.

## 6 Application: fMRI Inter-subject correlation (ISC) analysis

To demonstrate application of DEMINE and Meta-DEMINE on real data, we study the effectiveness of using DEMINE and Meta-DEMINE for Inter-subject Correlation (ISC) analysis of fMRI images.

Humans use language to effectively transmit brain representations among conspecifics. For example, after witnessing an event in the world, a speaker may use verbal communication to evoke neural representations reflecting that event in a listener’s brain [25]. The efficacy of this transmission, in terms of listener comprehension, is predicted by speaker–listener neural synchrony and synchrony among listeners [47]. To date, most work has measured brain-to-brain synchrony using inter-subject correlation (ISC); quantified as the Pearson product-moment correlation coefficient between response time series for corresponding voxels or regions of interest (ROIs) across individuals [27]. By modeling each subject’s neural responses using the responses of other subjects, ISC analyses provide novel insights. Unlike traditional fMRI analysis, which often rely on highly-controlled stimuli and trial averaging, ISC analyses are particularly well-suited to continuous, naturalistic paradigms, as they do not require an explicit model of the stimulus and are sensitive to evolving narrative context [26, 6]. However, Pearson correlation only captures the linear association between voxel-wise response time series across subjects. Although extensions of ISC analysis have used Granger causality [42] and dynamic time warping [44] to accommodate temporal asynchrony, it is not clear how best to circumvent these limitations. In this work, inspired by recent successes in mutual information estimation in machine learning[5], we propose data-efficient DEMINE and Meta-DEMINE for capturing more complex signatures of brain-to-brain coupling by using neural networks to encode continuous fMRI responses, we can learn nonlinear and higher-order inter-subject associations.

### 6.1 Dataset and Metrics

**New fMRI Dataset.** We apply the proposed model to a newly collected fMRI dataset with 40 participants (mean age = 23.3 years, SD = 8.9, range: 18–53; 27 female) listening to four spoken stories<sup>78</sup>. The stories were renditions of “Pie Man” and “Running from the Bronx” by Jim O’Grady [36, 37], “The Man Who Forgot Ray Bradbury” by Neil Gaiman [16], and “I Knew You Were Black” by Carol Daniel [8]; story durations were 7, 9, 14, and 13 minutes, respectively. After scanning, participants completed a questionnaire comprising 25–30 questions per story intended to measure narrative comprehension. The questionnaires included multiple choice, True/False, and fill-in-the-blank questions, as well as four additional subjective ratings per story. Functional and structural images were acquired using a 3T Siemens Prisma with a 64-channel head coil<sup>9</sup>. Briefly, functional images were acquired in an interleaved fashion using gradient-echo echo-planar imaging with a multiband acceleration factor of 3 (TR/TE = 1500/31 ms, resolution = 2.5 mm isotropic voxels, full brain coverage). All fMRI data were formatted according to the Brain Imaging Data Structure (BIDS) standard [22] and preprocessed using fMRIprep [10]<sup>10</sup>. Functional data were corrected for slice timing, head motion, and susceptibility distortion, and normalized to MNI space using nonlinear registration. Nuisance variables comprising head motion parameters, framewise displacement, linear and quadratic trends, sine/cosine bases for high-pass filtering (0.007 Hz), and six principal component time series from cerebrospinal fluid (CSF) and white matter were regressed out of the signal using AFNI [7].

The fMRI data were first partitioned into a seen set of 20 subjects and a unseen set of 20 separate subjects. We restricted our analysis to three subsets of voxels: an anatomically defined gray matter mask (GM; 22,541 voxels), as well as functionally-defined masks of high ISC voxels (ISC; 15,041 voxels) and dorsal Default-Mode Network voxels (dDMN; 3,940 voxels). All masks were defined in MNI space, and the ISC and dDMN masks were defined using independent data from previous studies [45]. The fMRI data comprise  $\mathcal{X} \in \mathbb{R}^{V_i \times T}$  for each subject, where  $V_i$ represents the flattened and masked voxel space and  $T$ represents the number of samples (TRs) during auditory stimulus presentation.

**Details on Dataset Collection** Functional and structural images were acquired using a 3T Siemens Magnetom Prisma with a 64-channel head coil. Functional, blood-oxygenation-level-dependent

<sup>7</sup>Two of the stories were told by a professional storyteller undergoing an fMRI scan; however, fMRI data for the speaker were not analyzed for the present work due to the head motion induced by speech production.

<sup>8</sup>The study was conducted in compliance with the Institutional Review Board of the University

<sup>9</sup>See Appendix for additional image acquisition details.

<sup>10</sup>See Appendix for additional preprocessing details.

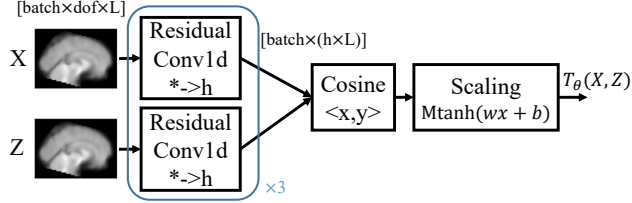


Figure 6: Network architecture for fMRI.

(BOLD) images were acquired in an interleaved fashion using gradient-echo echo-planar imaging with pre-scan normalization, fat suppression, a multiband acceleration factor of 3, and no in-plane acceleration: TR/TE = 1500/31 ms, flip angle = 67°, bandwidth = 2480 Hz/Px, resolution = 2.5 mm<sup>3</sup> isotropic voxels, matrix size = 96 x 96, FoV = 240 x 240 mm, 48 axial slices with roughly full brain coverage and no gap, anterior–posterior phase encoding. At the beginning of each scanning session, a T1-weighted structural scan was acquired using a high-resolution single-shot MPRAGE sequence with an in-plane acceleration factor of 2 using GRAPPA: TR/TE/TI = 2530/3.3/1100 ms, flip angle = 7°, resolution = 1.0 x 1.0 x 1.0 mm voxels, matrix size = 256 x 256, FoV = 256 x 256 x 176 mm, 176 sagittal slices, ascending acquisition, anterior–posterior phase encoding, no fat suppression, 5 min 53 s total acquisition time. At the end of each scanning session a T2-weighted structural scan was acquired using the same acquisition parameters and geometry as the T1-weighted structural image: TR/TE = 3200/428 ms, 4 min 40 s total acquisition time. A field map was acquired at the beginning of each scanning session, but was not used in subsequent analyses.

**Details on Dataset Preprocessing** Preprocessing was performed using fMRIPrep [10], a Nipype [21] based tool. T1-weighted images were corrected for intensity non-uniformity using N4 bias field correction [49] and skull-stripped using ANTs [3]. Nonlinear spatial normalization to the ICBM 152 Nonlinear Asymmetrical template version 2009c [14] was performed using ANTs. Brain tissue segmentation cerebrospinal fluid (CSF), white matter, and gray matter was was performed using FSL’s FAST [52]. Functional images were slice timing corrected using AFNI’s 3dTshift [7] and corrected for head motion using FSL’s MCFLIRT [29]. "Fieldmap-less" distortion correction was performed by co-registering each subject’s functional image to that subject’s intensity-inverted T1-weighted image [51] constrained with an average field map template [48]. This was followed by co-registration to the corresponding T1-weighted image using FreeSurfer’s boundary-based registration [23] with 9 degrees of freedom. Motion correcting transformations, field distortion correcting warp, BOLD-to-T1 transformation and T1-to-template (MNI) warp were concatenated and applied in a single step with Lanczos interpolation using ANTs. Physiological noise regressors were extracted applying aCompCor [4]. Six principal component time series were calculated within the intersection of the subcortical mask and the union of CSF and WM masks calculated in T1w space, after their projection to the native space of each functional run. Framewise displacement [40] was calculated for each functional run. Functional images were downsampled to 3 mm resolution. Nuisance variables comprising six head motion parameters (and their derivatives), framewise displacement, linear and quadratic trends, sine/cosine bases for high-pass filtering (0.007 Hz cutoff), and six principal component time series from an anatomically-defined mask of cerebrospinal fluid (CSF) and white matter were regressed out of the signal using AFNI’s 3dTproject [7]. Functional response time series were z-scored for each voxel.

## 6.2 Implementation Details

We study listener–listener coupling, where  $X$  and  $Z$  are a pair of synchronized window of  $L = 10$  TRs (15 seconds) with voxels selected using (ISC, dDMN, GM) listening to the same story. The neural network  $T_\theta(X, Z)$  is illustrated in Figure 6. It consists of two residual CNN encoders and a distance function. The residual CNN encoders first projects each frame of  $V_i$  voxels independently into a  $h = 256$ -dimensional vector. Subsequently 3 blocks of 1D residual convolution layers over the time dimension refines the representation. The distance function takes the  $h \times L$  representation of  $X$  and  $Z$ , computes their cosine distance, and passes it through a parameterized scaling layer  $M \times \tanh(w * \cos \langle \text{embed}(X), \text{embed}(Z) \rangle + b)$ , where  $w$  and  $b$  are parameters.

For DEMINE we use  $M = 5$ , learning rate  $\eta = 1 \times 10^{-3}$ , batch size 8192 over 20 iterations. For Meta-DEMINE we use  $M = 5$ , learning rate  $\eta = 1 \times 10^{-3}$ , batch size 128 over 80 iterations,

Table 4: Segment classification accuracy for NeuralMI versus Pearson’s correlation in 1 vs 1 and 1 vs rest (averaging over other subjects). Abbreviations: P: Pieman; F: Forgot; Br: Bronx; Bk: Black, MI: Mutual Information.

Classification Accuracy (%)	ISC Mask				dDMN Mask				GM Mask							
	P	F	Br	Bk	MI	P	F	Br	Bk	MI	P	F	Br	Bk	MI	
Chance	3.7	1.8	2.6	1.9	N/A	3.7	1.8	2.6	1.9	N/A	3.7	1.8	2.6	1.9	N/A	
Pearson’s r 1v1	11.1	6.8	9.4	9.6	N/A	6.5	2.7	5.1	3.8	N/A	9.4	4.6	8.0	6.2	N/A	
DEMINE 1v1	<b>26.3</b>	16.7	19.9	21.9	0.637	<b>7.2</b>	<b>3.0</b>	<b>5.6</b>	<b>4.7</b>	<b>0.035</b>	<b>26.2</b>	<b>17.2</b>	<b>21.3</b>	<b>23.5</b>	<b>0.610</b>	
Meta-DEMINE 1v1	26.2	<b>16.8</b>	<b>20.8</b>	<b>22.7</b>	<b>0.752</b>	5.8	2.9	4.9	4.1	0.031	-	-	-	-	-	
Pearson’s r 1vR	35.0	20.4	25.8	31.5	N/A	14.8	6.4	<b>11.8</b>	9.9	N/A	31.3	16.8	26.6	24.2	N/A	
DEMINE 1vR	42.8	28.0	32.8	35.9	0.637	<b>16.5</b>	<b>7.9</b>	11.6	<b>12.0</b>	<b>0.035</b>	<b>49.8</b>	<b>29.6</b>	<b>33.9</b>	<b>38.1</b>	<b>0.610</b>	
Meta-DEMINE 1vR	<b>47.2</b>	<b>32.5</b>	<b>39.9</b>	<b>41.0</b>	<b>0.752</b>	13.7	7.9	8.2	8.9	0.031	-	-	-	-	-	

meta learning rate  $\eta_{\text{meta}} = 3 \times 10^{-4}$ , with BPTT-based meta-optimization over 5000 iterations. For DEMINE we report results on ISC, dDMN and GM masks. For Meta-DEMINE we report results on ISC and dDMN masks, while GM does not fit into the GPU memory due to the high memory consumption of BPTT.

### 6.3 Results

We study the MI estimation and between-subject time-segment classification of DEMINE and Meta-DEMINE comparing with Pearson’s correlation commonly used in ISC analysis.

**Quantitative Results.** For the learned  $T_\theta(X, Z)$ , we use between-subject time-segment classification (BSC) for evaluation [28, 24]. Each video is divided into  $K$  non-overlapping  $L = 10TR$  time segments. The BSC task is 1) one versus one: given a time segment  $x$  from an individual, retrieve the corresponding time segment  $z$  from another individual out of the  $K$  possible segments; 2) one versus rest: retrieve the corresponding time segment  $z$  of an individual given a group of time segments  $x$  excluding that individual. Performance is measured by top-1 retrieval accuracy.

For DEMINE, we compute score  $T_\theta(X, Z)$  for each pair of  $X$  and  $Z$  for one versus one, and average over  $X$  for one versus all. For Pearson correlation,  $\rho(X, Z)$  for one vs one, and compute  $\rho(\bar{X}, Z)$  for one versus all, where  $\bar{X}$  is mean of  $X$  from subjects different than  $Z$ .<sup>11</sup> Results are shown in Tab. 4. DEMINE consistently outperforms Pearson correlation on ISC, dDMN and GM for all 4 stories. Meta-DEMINE greatly improves both accuracy and mutual information estimation on the ISC mask. The low performance on dDMN mask is likely due to BPTT optimization unable to decrease the meta learning loss, which could be improved by further improvements on the optimization algorithm.

For mutual information estimation, DEMINE predicts 0.637, 0.035 and 0.610 nats of mutual information communicated over 10 TRs (15 seconds), for ISC, DMN and GM masks respectively.

**Qualitative Results.** Fig. 7 (top) visualizes voxels that are important to  $T(x, z)$  using their gradient magnitude variance for the ISC, dDMN, and GM masks. The models focuses on auditory regions functionally important for perceiving the story stimulus.

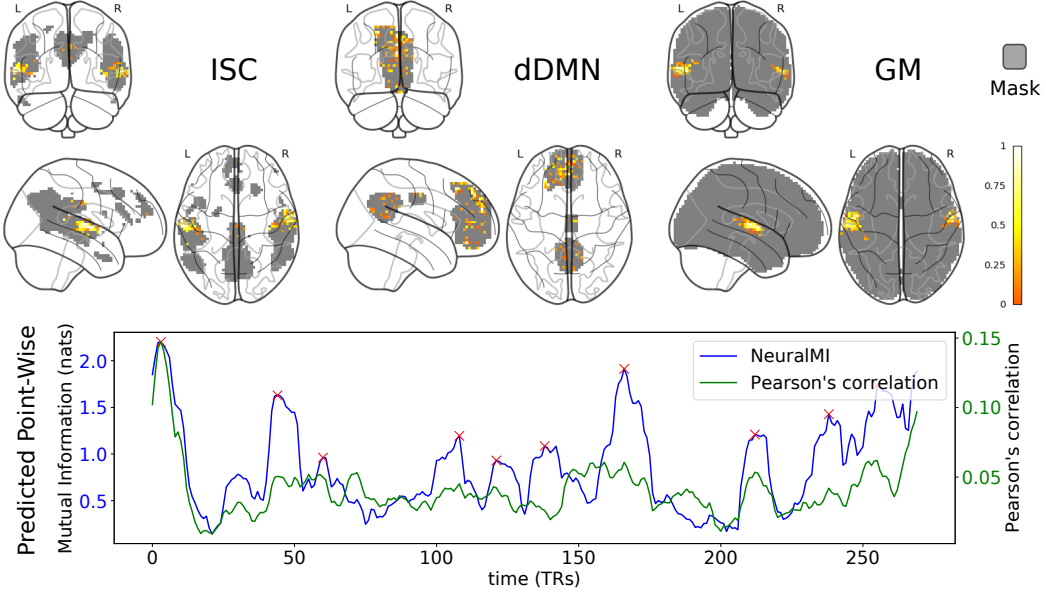
Fig. 7 (bottom) plots the  $T(x, z)$  and intersubject Pearson correlations over time for "Pie Man" using the ISC mask, a sliding window size  $L = 10$ , using the one vs rest scores averaged over all subjects. NeuralMI yields more distinctive peaks.

We identify the peaks in DEMINE for "Pie Man" (with Pearson correlations) over time, then locate the story transcriptions in the  $L = 10TRs$  (15 seconds) window corresponding to the peak:

- 4: "...toiled for The Ram, uh, Fordham University’s student newspaper. And one day, I’m walking toward the campus center and out comes the elusive Dean McGowen, architect of a policy to replace traditionally ..."
- 45: "The Dean is covered with cream. So I give him a moment, then I say, ‘Dean McGowen, would you care to comment on this latest attack?’ And he says, ‘Yes, I would care to comment. ...’"
- 109: "...which makes no sense. Fordham was a Catholic school and we all thought Latin was classy so, that’s what I used. And when I finished my story, I, I raced back to Dwyer and I showed it to him and he read it and he said ..."

<sup>11</sup>Empirically  $\rho(\bar{X}, Z)$  performs better than  $\sum_X \rho(X, Z)$ . For Pearson correlation over multiple voxels, we treat samples from different voxels as i.i.d. samples from a single sequence and compute Pearson correlation.

Figure 7: Top: Top contributing voxels in the learned  $T_\theta(X, Z)$  by gradient magnitude  $\mathbb{E}_X (\frac{\partial T}{\partial X_i})^2$ . Auditory region is highlighted for ISC and GM masks (best in color). Bottom: Evaluation on the "Pie Man" dataset using the ISC mask showing our approach  $T_\theta(X, Z)$  versus Pearson correlation over time in the one versus rest case averaged over 20 test subjects.



- 122: "Few days later, I get a letter. I opened it up and it says, "Dear Jim, good story. Nice details. If you want to see me again in action, be on the steps of Duane Library ..."
- 139: "...out comes student body president, Sheila Biel. And now, Sheila Biel was different from the rest of us flannel-shirt wearing, part-time-job working, Fordham students. Sheila was..."
- 167: "Pie Man emerged from behind a late night library drop box, made his delivery, and fled away, crying, "Ego sum non una bestia." And that's what I reported in my story..."
- 213: "...that there was a question about whether she even knew if I existed. So I saw her there and made a mental note to do nothing about it, and then I went to the bar and ordered a drink, and I felt a, a tap on my shoulder. I turned around, and it was her...."
- 239: "And wasn't I really Pie Man? Hadn't I brought him into existence? Didn't she only know about him because of me? But actually ..."
- 256: "I said, "Yes, Angela, I am Pie Man.' And she looked at me and she said, 'Oh, good. I was hoping you'd say that ..."

We hypothesize that the scripts associated with the peaks may capture points when listeners pay more attention, resulting in the Signal-to-Noise Ratio (SNR) of fMRI scans being enhanced.

## 7 Conclusions

In this work, we developed DEMINE and Meta-DEMINE to use neural networks for mutual information estimation with high accuracy and data-efficiency. We conduct synthetic experiments to validate the proposed neural mutual information estimators, and apply them to fMRI data for improving accuracy of inter-subject correlation analysis. We show that our neural mutual information estimators DEMINE and Meta-DEMINE are effective in analyzing non-linear dependency in high-dimensional fMRI signals where traditional correlation-based analysis are unable to capture. Our results suggest a greater avenue of using neural networks and meta learning to improve mutual information analysis and applying deep learning-based information theory tools to enhancing the analysis of information processing in the brain.

Model-agnostic high-confidence MI lower bound estimation approaches – including *MINE*, DEMINE and Meta-DEMINE – are limited to estimating small MI lower bounds up to  $O(\log n)$  as pointed out in [34], where  $n$  is the number of samples. For DEMINE and Meta-DEMINE, estimating higher MI lower bounds requires larger  $M$ , which in turn will reduce estimation confidence exponentially. When quantitatively measuring strong dependency, cross-entropy may be measured with higher confidence as pointed out in [34], where as DEMINE and Meta-DEMINE are useful for performing a statistical test of dependency and estimation of small MI lower bounds.

## Acknowledgments

This work is funded by DARPA FA8750-18-C-0213. The views, opinions, and/or conclusions contained in this paper are those of the author and should not be interpreted as representing the official views or policies, either expressed or implied of the DARPA or the DoD.

## References

- [1] D. B. F. Agakov. The IM algorithm: a variational approach to information maximization. *Advances in Neural Information Processing Systems*, 16:201, 2004.
- [2] I. Ahmad and P.-E. Lin. A nonparametric estimation of the entropy for absolutely continuous distributions (corresp.). *IEEE Transactions on Information Theory*, 22(3):372–375, 1976.
- [3] B. B. Avants, C. L. Epstein, M. Grossman, and J. C. Gee. Symmetric diffeomorphic image registration with cross-correlation: evaluating automated labeling of elderly and neurodegenerative brain. *Medical Image Analysis*, 12(1):26–41, 2008.
- [4] Y. Behzadi, K. Restom, J. Liau, and T. T. Liu. A component based noise correction method (CompCor) for BOLD and perfusion based fMRI. *NeuroImage*, 37(1):90–101, 2007.
- [5] M. I. Belghazi, A. Baratin, S. Rajeshwar, S. Ozair, Y. Bengio, D. Hjelm, and A. Courville. Mutual information neural estimation. In *International Conference on Machine Learning*, pages 530–539, 2018.
- [6] A. Ben-Yakov, C. J. Honey, Y. Lerner, and U. Hasson. Loss of reliable temporal structure in event-related averaging of naturalistic stimuli. *NeuroImage*, 63(1):501–506, 2012.
- [7] R. W. Cox. AFNI: software for analysis and visualization of functional magnetic resonance neuroimages. *Computers and Biomedical research*, 29(3):162–173, 1996.
- [8] C. Daniel. I knew you were black. <https://themoth.org/stories/i-knew-you-were-black>, 2018. Accessed: 2018-10-12.
- [9] G. A. Darbellay and I. Vajda. Estimation of the information by an adaptive partitioning of the observation space. *IEEE Transactions on Information Theory*, 45(4):1315–1321, May 1999.
- [10] O. Esteban, C. Markiewicz, R. W. Blair, C. Moodie, A. I. Isik, A. Erramuzpe Aliaga, J. Kent, M. Goncalves, E. DuPre, M. Snyder, H. Oya, S. Ghosh, J. Wright, J. Durnez, R. Poldrack, and K. J. Gorgolewski. FMRIPrep: a robust preprocessing pipeline for functional MRI. *bioRxiv*, 2018.
- [11] C. Finn, P. Abbeel, and S. Levine. Model-agnostic meta-learning for fast adaptation of deep networks. In *Proceedings of the 34th International Conference on Machine Learning, ICML 2017, Sydney, NSW, Australia, 6–11 August 2017*, pages 1126–1135, 2017.
- [12] C. Finn, K. Xu, and S. Levine. Probabilistic model-agnostic meta-learning. In *Advances in Neural Information Processing Systems*, pages 9537–9548, 2018.
- [13] C. Finn, T. Yu, T. Zhang, P. Abbeel, and S. Levine. One-shot visual imitation learning via meta-learning. In *Conference on Robot Learning*, pages 357–368, 2017.
- [14] V. S. Fonov, A. C. Evans, R. C. McKinstry, C. Almlie, and D. Collins. Unbiased nonlinear average age-appropriate brain templates from birth to adulthood. *NeuroImage*, (47):S102, 2009.
- [15] A. M. Fraser and H. L. Swinney. Independent coordinates for strange attractors from mutual information. *Phys. Rev. A*, 33:1134–1140, Feb 1986.
- [16] N. Gaiman. The man who forgot ray bradbury. <https://soundcloud.com/neilgaiman/the-man-who-forgot-ray-bradbury>, 2018. Accessed: 2018-10-12.
- [17] W. Gao, S. Kannan, S. Oh, and P. Viswanath. Estimating mutual information for discrete-continuous mixtures. In *Advances in Neural Information Processing Systems*, pages 5986–5997, 2017.
- [18] W. Gao, S. Oh, and P. Viswanath. Demystifying fixed  $k$ -nearest neighbor information estimators. *IEEE Transactions on Information Theory*, 64(8):5629–5661, 2018.
- [19] X. Glorot and Y. Bengio. Understanding the difficulty of training deep feedforward neural networks. In *In Proceedings of the International Conference on Artificial Intelligence and Statistics (AISTATS’10). Society for Artificial Intelligence and Statistics*, 2010.
- [20] I. J. Goodfellow. NIPS 2016 tutorial: Generative adversarial networks. *CoRR*, abs/1701.00160, 2017.
- [21] K. Gorgolewski, C. Burns, C. Madison, D. Clark, Y. Halchenko, M. Waskom, and S. Ghosh. Nipype: a flexible, lightweight and extensible neuroimaging data processing framework in python. *Frontiers in Neuroinformatics*, 5:13, 2011.
- [22] K. J. Gorgolewski, T. Auer, V. D. Calhoun, R. C. Craddock, S. Das, E. P. Duff, G. Flandin, S. S. Ghosh, T. Glatard, Y. O. Halchenko, et al. The brain imaging data structure, a format for organizing and describing outputs of neuroimaging experiments. *Scientific Data*, 3:160044, 2016.
- [23] D. N. Greve and B. Fischl. Accurate and robust brain image alignment using boundary-based registration. *NeuroImage*, 48(1):63–72, 2009.

[24] J. S. Guntupalli, M. Hanke, Y. O. Halchenko, A. C. Connolly, P. J. Ramadge, and J. V. Haxby. A model of representational spaces in human cortex. *Cerebral Cortex*, 26(6):2919–2934, 2016.

[25] U. Hasson, A. A. Ghazanfar, B. Galantucci, S. Garrod, and C. Keysers. Brain-to-brain coupling: a mechanism for creating and sharing a social world. *Trends in cognitive sciences*, 16(2):114–121, 2012.

[26] U. Hasson, R. Malach, and D. J. Heeger. Reliability of cortical activity during natural stimulation. *Trends in Cognitive Sciences*, 14(1):40–48, 2010.

[27] U. Hasson, Y. Nir, I. Levy, G. Fuhrmann, and R. Malach. Intersubject synchronization of cortical activity during natural vision. *Science*, 303(5664):1634–1640, 2004.

[28] J. V. Haxby, J. S. Guntupalli, A. C. Connolly, Y. O. Halchenko, B. R. Conroy, M. I. Gobbini, M. Hanke, and P. J. Ramadge. A common, high-dimensional model of the representational space in human ventral temporal cortex. *Neuron*, 72(2):404–416, 2011.

[29] M. Jenkinson, P. Bannister, M. Brady, and S. Smith. Improved optimization for the robust and accurate linear registration and motion correction of brain images. *NeuroImage*, 17(2):825–841, 2002.

[30] T. Kim, J. Yoon, O. Dia, S. Kim, Y. Bengio, and S. Ahn. Bayesian model-agnostic meta-learning. *arXiv preprint arXiv:1806.03836*, 2018.

[31] D. P. Kingma and J. Ba. Adam: A method for stochastic optimization. *arXiv preprint arXiv:1412.6980*, 2014.

[32] A. Kraskov, H. Stogbauer, and P. Grassberger. Estimating mutual information. *Physical review E*, 2004.

[33] D. Maclaurin, D. Duvenaud, and R. Adams. Gradient-based hyperparameter optimization through reversible learning. In *International Conference on Machine Learning*, pages 2113–2122, 2015.

[34] D. McAllester and K. Statos. Formal limitations on the measurement of mutual information. *arXiv preprint arXiv:1811.04251*, 2018.

[35] X. Nguyen, M. J. Wainwright, and M. I. Jordan. Estimating divergence functionals and the likelihood ratio by convex risk minimization. *IEEE Transactions on Information Theory*, 56(11):5847–5861, 2010.

[36] J. O’Grady. Pie Man. <https://themoth.org/stories/pie-man>, 2018. Accessed: 2018-10-12.

[37] J. O’Grady. Running from the Bronx. <https://soundcloud.com/the-story-collider/jim-ogrady-running-from-the>, 2018. Accessed: 2018-10-12.

[38] H. Pham, M. Guan, B. Zoph, Q. Le, and J. Dean. Efficient neural architecture search via parameter sharing. In *International Conference on Machine Learning*, pages 4092–4101, 2018.

[39] B. Poole, S. Ozair, A. van den Oord, A. A. Alemi, and G. Tucker. On variational lower bounds of mutual information. In *Bayesian Deep Learning Workshop, NeurIPS*, 2018.

[40] J. D. Power, A. Mitra, T. O. Laumann, A. Z. Snyder, B. L. Schlaggar, and S. E. Petersen. Methods to detect, characterize, and remove motion artifact in resting state fMRI. *NeuroImage*, 84:320–341, 2014.

[41] T. Salimans, J. Ho, X. Chen, S. Sidor, and I. Sutskever. Evolution strategies as a scalable alternative to reinforcement learning. *arXiv preprint arXiv:1703.03864*, 2017.

[42] M. B. Schippers, A. Roebroeck, R. Renken, L. Nanetti, and C. Keysers. Mapping the information flow from one brain to another during gestural communication. *Proceedings of the National Academy of Sciences*, page 201001791, 2010.

[43] F. Sehnke, C. Osendorfer, T. Rückstieß, A. Graves, J. Peters, and J. Schmidhuber. Parameter-exploring policy gradients. *Neural Networks*, 23(4):551–559, 2010.

[44] L. J. Silbert, C. J. Honey, E. Simony, D. Poeppel, and U. Hasson. Coupled neural systems underlie the production and comprehension of naturalistic narrative speech. *Proceedings of the National Academy of Sciences*, 111(43):E4687–E4696, 2014.

[45] E. Simony, C. J. Honey, J. Chen, O. Lositsky, Y. Yeshurun, A. Wiesel, and U. Hasson. Dynamic reconfiguration of the default mode network during narrative comprehension. *Nature Communications*, 7:12141, 2016.

[46] J. Snell, K. Swersky, and R. Zemel. Prototypical networks for few-shot learning. In *Advances in Neural Information Processing Systems*, pages 4077–4087, 2017.

- [47] G. J. Stephens, L. J. Silbert, and U. Hasson. Speaker–listener neural coupling underlies successful communication. *Proceedings of the National Academy of Sciences*, 107(32):14425–14430, 2010.
- [48] J. M. Treiber, N. S. White, T. C. Steed, H. Bartsch, D. Holland, N. Farid, C. R. McDonald, B. S. Carter, A. M. Dale, and C. C. Chen. Characterization and correction of geometric distortions in 814 diffusion weighted images. *PLOS ONE*, 11(3):e0152472, 2016.
- [49] N. J. Tustison, B. B. Avants, P. A. Cook, Y. Zheng, A. Egan, P. A. Yushkevich, and J. C. Gee. N4itk: improved n3 bias correction. *IEEE Transactions on Medical Imaging*, 29(6):1310–1320, June 2010.
- [50] O. Vinyals, C. Blundell, T. Lillicrap, D. Wierstra, et al. Matching networks for one shot learning. In *Advances in neural information processing systems*, pages 3630–3638, 2016.
- [51] S. Wang, D. J. Peterson, J. C. Gatenby, W. Li, T. J. Grabowski, and T. M. Madhyastha. Evaluation of field map and nonlinear registration methods for correction of susceptibility artifacts in diffusion mri. *Frontiers in Neuroinformatics*, 11:17, 2017.
- [52] Y. Zhang, M. Brady, and S. Smith. Segmentation of brain MR images through a hidden markov random field model and the expectation-maximization algorithm. *IEEE Transactions on Medical Imaging*, 20(1):45–57, 2001.